

# Topological superconducting transition driven by time-reversal-symmetry breaking

Jing Wang\*

Department of Physics, Tianjin University, Tianjin 300072, P. R. China

(Dated: March 15, 2021)

Three-dimensional line-nodal superconductors exhibit nontrivial topology, which is protected by the time-reversal symmetry. Here we investigate four types of short-range interaction between the gapless line-nodal fermionic quasiparticles by carrying renormalization group analysis. We find that such interactions can induce the dynamical breaking of time-reversal symmetry, which alters the topology and might lead to six possible distinct superconducting states, distinguished by the group representations. After computing the susceptibilities for all the possible phase-transition instabilities, we establish that the superconducting pairing characterized by  $id_{xz}$ -wave gap symmetry is the leading instability in noncentrosymmetric superconductors. Appropriate extension of this approach is promising to pick out the most favorable superconducting pairing during similar topology-changing transition in the polar phase of  $^3\text{He}$ .

PACS numbers: 74.20.Mn, 74.20.Rp

## I. INTRODUCTION

Superconductivity has been studied for more than one century. Ordinary phonon-mediated superconductors have an isotropic  $s$ -wave superconducting (SC) gap, which suppresses fermionic excitations at low energies [1, 2]. Cuprate superconductors possess an anisotropic  $d_{x^2-y^2}$ -wave SC gap [3] that hosts four nodal points. In some cases, pure  $d_{x^2-y^2}$ -wave SC state may undergo a quantum phase transition (QPT), entering into another SC state which has a distinct gap symmetry [4]. The quantum criticality of such a QPT is governed by the interaction between nodal quasiparticles and quantum fluctuation of new SC order parameter, and the proximity to  $d_{x^2-y^2} + id_{xy}$ -wave SC phase was argued [4] to account for the observed marginal Fermi liquid behavior in optimally doped  $\text{Bi}_2\text{Sr}_2\text{CaCu}_2\text{O}_{8+\delta}$  [5].

Experiments reveal that, some three-dimensional (3D) heavy fermion compounds [6–8] and iron-based superconductors [9, 10] exhibit a line-shape nodal structure in the SC gap. Examples are  $\text{CePt}_3\text{Si}$  [6, 7],  $\text{UCoGe}$  [8], and  $\text{Ba}(\text{Fe}_{1-x}\text{Co}_x)_2\text{As}_2$  [9, 10]. Due to the presence of gap vanishing lines, there are fermionic excitations even at ultra-low energies [11, 12]. Different from 2D point-nodal superconductors, 3D line-nodal superconductor may host striking topological SC state [13]. Of particular interest is the nodal centrosymmetric superconductor in which the absence of inversion symmetry allows for the mixing of even and odd parities.

The stability of the topological SC state in nodal noncentrosymmetric superconductors is protected by the time-reversal ( $\mathcal{T}$ ) symmetry [13]. This topology will be changed once  $\mathcal{T}$ -symmetry is broken [14].  $\mathcal{T}$ -symmetry breaking ( $\mathcal{TSB}$ ) drives the system into a distinct SC phase. This transition is characterized by the simultaneous changes of both symmetry and topology, at which

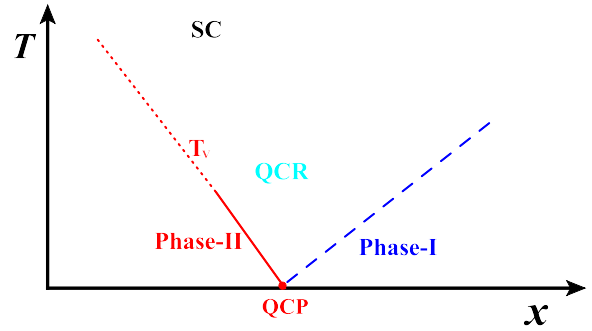


FIG. 1: (Color online) Schematic phase diagram on  $x$ - $T$  plane, where  $x$  is non-thermal tuning parameter and  $T$  temperature. A putative QCP separates two distinct superconducting phases, i.e., Phases I and II.  $\mathcal{T}$ -symmetry is respected in Phase I and broken in Phase II.

the conventional symmetry-breaking is a crucial ingredient in reconstructing the band structure and leading to topological changes [15–17]. A schematic phase diagram is presented in Fig. 1. Two distinct SC phases, i.e., Phase I and Phase II, are separated by a quantum critical point (QCP) in the  $x$ -axis. Phase I is a  $\mathcal{T}$ -symmetry protected topological SC phase, whereas Phase II a  $\mathcal{TSB}$  SC phase. The gap structure of  $\mathcal{TSB}$  SC state is not unique, and should be specified by the representations of the underlying group of the system. For instance, for a system described by  $C_{4v} \times \mathcal{T} \times \mathcal{P}$  group, where  $C_{4v}$  is the tetragonal symmetry (inversion-symmetry broken) and  $\mathcal{P}$  is particle-hole symmetry, there are six possible  $\mathcal{TSB}$  SC states [14], distinguished by the gap structure. The order parameters for these six states are summarized in Table I. As it concerns the question on whether the phases shown in Fig. 1 are topological or not, that crucially depends upon the corresponding order parameters and the specific broken symmetries. We therefore are allowed to extract the non-trivial changes of topological phases from investigating the related traditional symmetry breakings [14–17].

\*E-mail address: jing\_wang@tju.edu.cn

TABLE I: There are six different  $\mathcal{TSB}$  SC phases, which have different gap structures and different coupling matrices for the coupling between fermions and source terms. These  $\mathcal{TSB}$  SC phases with inversion-symmetry breaking are associated with distinct sorts of continuum representations (coupling matrices) near their nodal lines owing to the qualitative difference of nodal structures [14]. There are six possible states: 1) SC-I (*is*-pairing); 2) SC-II (*ig*-pairing); 3) SC-III (*id<sub>x<sup>2</sup>-y<sup>2</sup></sub>*-pairing); 4) SC-IV (*id<sub>xy</sub>*-pairing); 5) SC-V (*id<sub>xz</sub>*-pairing); and 6) SC-VI (*id<sub>yz</sub>*-pairing).

Order parameter ( $\Delta_i$ )	SC-I	SC-II	SC-III	SC-IV	SC-V	SC-VI
Coupling matrices ( $\mathcal{M}_i$ )	$\tau^y$	$\frac{1}{4} \sin(4\theta_{\mathbf{k}})\tau^y$	$\cos(2\theta_{\mathbf{k}})\tau^y$	$\frac{1}{2} \sin(2\theta_{\mathbf{k}})\tau^y$	$\cos(\theta_{\mathbf{k}})\tau^y$	$\sin(\theta_{\mathbf{k}})\tau^y$

Two interesting questions arise naturally. What is the driving force of  $\mathcal{TSB}$ ? How could one determine the most favorable  $\mathcal{TSB}$  SC phase among the six candidates?

To answer these questions, in this paper we will consider four types of short-range interactions between the gapless fermionic quasiparticles excited near the SC gap nodal lines. After performing one-loop renormalization group (RG) analysis [18–20], we derive the coupled flow equations of all the model parameters, including the fermion velocities and the coupling constants. Based on the RG results, we show that all the four coupling constants diverge at low energies. This indicates that the system becomes unstable and should enter into a distinct new phase. This new phase could be one of the six  $\mathcal{TSB}$  SC phases.

It should be noted that RG flows of coupling parameters do not provide sufficient information to determine the leading ordering tendency [21]. To find out the dominant instability, we will study all the possible ordered phases (restricted to the charge channel), and evaluate the corresponding susceptibilities for each ordered phase based on the RG flow equations of model parameters. Our analytical and numerical calculations indicate that, the leading instability caused by four-fermion couplings is the emergence of  $\mathcal{TSB}$  SC order. Among the six candidates, the  $\mathcal{TSB}$  SC state with *id<sub>xz</sub>*-wave symmetry is the most favorable. It is also of particular interest to generalize our method to identify the leading instability of the analogous topological  $\mathcal{TSB}$ -driven transition in the polar phase of  $^3\text{He}$  [22].

## II. EFFECTIVE THEORY AND RG ANALYSIS

We consider 3D line-nodal noncentrosymmetric superconductors characterized by the symmetry group  $\mathcal{G} = C_{4v} \times \mathcal{T} \times \mathcal{P}$ . The generalization to other groups is straightforward. The low-energy mean-field Hamiltonian of this system is formally written as [13, 14]

$$H_0 = \sum_{\mathbf{k}} \Psi_{\mathbf{k}}^\dagger [h(\mathbf{k})\tau^z + \Delta(\mathbf{k})\tau^x] \Psi_{\mathbf{k}}, \quad (1)$$

where the four-component spinor is  $\Psi_{\mathbf{k}}^\dagger = (\psi_{\mathbf{k}}^\dagger, i\sigma^y \psi_{-\mathbf{k}}^T)$  with  $\psi_{\mathbf{k}}^\dagger = (c_{\mathbf{k}\uparrow}^*, c_{\mathbf{k}\downarrow}^*)$ . Pauli matrices  $\tau^{x,y,z}$  and  $\sigma^{x,y,z}$  act in the particle-hole space and spin space, respectively.

The  $\tau^z$  term captures the fermionic degrees of freedom in the non-SC phase [14, 23, 24]. The energy spectrum is given by  $h(\mathbf{k}) = \epsilon(\mathbf{k}) - \mu + \alpha \mathbf{l}(\mathbf{k}) \cdot \sigma$ , where the kinetic energy  $\epsilon(\mathbf{k}) = -2t(\cos k_x + \cos k_y + \cos k_z)$ . Spin-orbital coupling is included by introducing the parameter  $\alpha$ . The  $\tau^x$ -term corresponds to the SC pairing, and the SC order parameter has the form [14]  $\Delta(\mathbf{k}) = \Delta_s + \Delta_t \mathbf{d}(\mathbf{k}) \cdot \sigma$ , where  $\Delta_s$  is an even-parity spin-singlet gap and  $\Delta_t$  an odd-parity spin-triplet gap. The pairing term is chosen to be along the same direction as that of spin-orbital coupling, i.e.,  $\mathbf{l}(\mathbf{k}) = \mathbf{d}(\mathbf{k})$ . The amplitudes  $\Delta_s$  and  $\Delta_t$  are taken to be real and positive due to  $\mathcal{T}$ -symmetry [14].

As aforementioned,  $\mathcal{TSB}$  alters the topology of the SC state.  $\mathcal{TSB}$  can be realized by adding an extra  $\tau^y$  term. In Ref. [14], Han *et al.* considered one specific four-fermion coupling  $(\Psi^\dagger \tau^y \Psi)^2$  and made a mean-field analysis to generate  $\tau^y$  term. This coupling is certainly not the only possibility, and other four-fermion couplings could be present. To make an unbiased judgement, we consider the following four couplings

$$H_{\text{int}} = \sum_{i=0}^3 \int d^3 \mathbf{x} u_i (\Psi^\dagger \gamma^i \Psi)^2, \quad (2)$$

where  $u_{0,1,2,3}$  are coupling constants,  $\gamma^0 \equiv \tau^0 = I_{2 \times 2}$ , and  $\gamma^{1,2,3} \equiv \tau^{x,y,z}$ . Mean-field treatment ignores the quantum fluctuations and cannot determine the relative importance of the above four possible couplings. Here we go beyond the mean-field level, and take into account the quantum fluctuations by using the RG techniques. It will become clear that, RG not only selects out the most important coupling, but also pins down the leading ordering instability.

One can verify [13, 14] that the above SC gap has a line-node structure. Gapless fermions are excited around the nodal lines. To obtain the low-energy continuum limit, we follow Ref. [14] and implement the approximations  $\epsilon(\mathbf{k}) \rightarrow \frac{\mathbf{k}^2}{2m}$  with  $m = \frac{1}{2t}$  and  $\vec{l}(\mathbf{k}) \approx (k_x, k_y, 0) = \mathbf{k}_\perp$ . It suffices to focus on the upper nodal-ring, since the lower nodal-ring is equivalent. Gathering the effective free Hamiltonian  $H_0 \sim \Psi_{\mathbf{k}}^\dagger (v_z \delta k_z \tau^z + v_p \delta k_\perp \tau^x) \Psi_{\mathbf{k}}$  and interactions (2) gives rise to the total low-energy effective action

$$S_{\text{eff}} = \int_{\mathbf{k}, \omega} \Psi_{\mathbf{k}, \omega}^\dagger (-i\omega + v_z \delta k_z \tau^z + v_p \delta k_\perp \tau^x) \Psi_{\mathbf{k}, \omega}$$

$$\begin{aligned}
& + \sum_{i=0}^3 u_i \prod_{j=1}^4 \int_{\mathbf{k}_j, \omega_j} \Psi_{\mathbf{k}_1, \omega_1}^\dagger \gamma^i \Psi_{\mathbf{k}_2, \omega_2} \Psi_{\mathbf{k}_3, \omega_3}^\dagger \gamma^i \Psi_{\mathbf{k}_4, \omega_4} \\
& \times \delta^{(3)}(\mathbf{k}_1 + \mathbf{k}_2 - \mathbf{k}_3 - \mathbf{k}_4) \delta(\omega_1 + \omega_2 - \omega_3 - \omega_4). \quad (3)
\end{aligned}$$

The free fermion propagator is given by  $G_0^{-1}(k) = -i\omega + v_z \delta k_z \tau^z + v_p \delta k_\perp \tau^x$ . Throughout the following calculations, we focus on the limit of  $|k| \ll k_F$  (with the size of nodal ring  $k_F$ ) and as such adopt the approximation for the form factor  $\mathcal{F}(\mathbf{k}) \rightarrow \mathcal{F}(\theta_{\mathbf{k}})$ . This allows us to adopt the approximations  $\sin k_x \approx \cos \theta_{\mathbf{k}}$ ,  $\sin k_y \approx \sin \theta_{\mathbf{k}}$ ,  $\cos k_x - \cos k_y \approx \cos 2\theta_{\mathbf{k}}$ , and  $\sin k_z \approx u^z$ . We use  $v_z$  to denote the fermion velocity along  $z$ -axis, and  $v_p$  the one within the  $x$ - $y$  plane. In addition, we now can invoke the following approximation [14]

$$\int_{\mathbf{k}, \omega} \equiv \int \frac{d^3 k d\omega}{(2\pi)^4} \approx \int \frac{d\delta k_z}{2\pi} \int k_F \frac{d\delta k_\perp}{2\pi} \int \frac{d\theta_{\mathbf{k}}}{2\pi} \int \frac{d\omega}{2\pi}, \quad (4)$$

with  $\delta k_\perp^2 = \delta k_x^2 + \delta k_y^2$ .

The RG flow equations of fermion velocities and four-fermion interaction parameters are [20, 25–27]

$$\frac{dv_z}{dl} = \frac{1}{4\pi v_z v_p} v_z (u_0 + u_3), \quad (5)$$

$$\frac{dv_p}{dl} = \frac{1}{4\pi v_z v_p} v_p (u_0 + u_1), \quad (6)$$

$$\frac{du_0}{dl} = \frac{8}{16\pi v_z v_p} [u_0^2 + u_2(\mathcal{E}u_3 + \mathcal{F}u_1)], \quad (7)$$

$$\begin{aligned}
\frac{du_1}{dl} = & \frac{1}{16\pi v_z v_p} [u_1(1 + \mathcal{F} - \mathcal{E})(u_0 + 3u_1 - u_2 - u_3) \\
& + 8u_1(u_0 + \mathcal{F}u_3) - 4u_2u_3], \quad (8)
\end{aligned}$$

$$\begin{aligned}
\frac{du_2}{dl} = & \frac{1}{16\pi v_z v_p} [u_2(1 + \mathcal{F} + \mathcal{E})(u_0 - u_1 + 3u_2 - u_3) \\
& + 8u_2(u_0 + \mathcal{E}u_1 + \mathcal{F}u_3) - 4u_1u_3], \quad (9)
\end{aligned}$$

$$\begin{aligned}
\frac{du_3}{dl} = & \frac{1}{16\pi v_z v_p} [u_3(1 - \mathcal{F} + \mathcal{E})(u_0 - u_1 - u_2 + 3u_3) \\
& + 8u_3(u_0 + \mathcal{E}u_1) - 4u_1u_2]. \quad (10)
\end{aligned}$$

Here, the coefficients  $\mathcal{E}$  and  $\mathcal{F}$  as well as the one-loop calculations of vertex corrections are presented in Appendix A.

### III. RESULTS AND DISCUSSIONS

After solving the flow equations (5)-(10), we find that all of the four parameters  $u_i$  diverge at certain critical scale  $l_c$ , no matter whether the starting values of  $v_z$  and  $v_p$  are equal or not. The results are shown in the inset of Fig. 2. The four-fermion couplings are thus marginally relevant at low energies [20] and can lead to some kinds of phase-transition instability [16, 17, 21, 28, 29].

The parameters  $u_i$  go to infinity at different speeds. Their relative importance [16, 17, 30] can be distinguished by re-scaling all the parameters with respect to

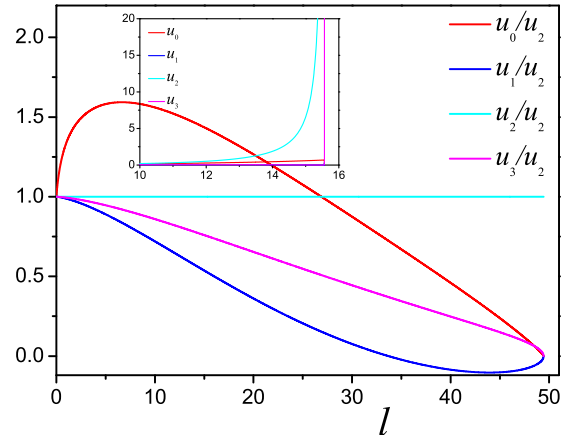


FIG. 2: (Color online) Evolutions of  $u_i/u_2$  ( $i = 0, 1, 2, 3$ ) with  $\frac{v_z(0)}{v_p(0)} = 5$  and  $u_i(0) = 10^{-4}$  and  $u_i$  (inset) with  $u_i(0) = 10^{-4}$  and  $v_z(0) = v_p(0) = 0.001$ . This fixed point is independent of the initial values of fermion velocities and coupling constants (the curves for  $u_1$  and  $u_3$  coincide).

one of them (no sign change). Here, we choose to analyze the energy-dependence of the ratios  $u_i/u_2$ . At the outset, we let  $v_z$  be equal to  $v_p$  at  $l = 0$ . Numerical analysis reveals that the re-scaled parameters  $u_i/u_2$  inescapably flow to  $(u_0, u_1, u_2, u_3)/u_2 \approx (0, 0, 1, 0)$ . This result is independent of the bare values of  $u_i(0)$ ,  $v_z(0)$ , and  $v_p(0)$ , as illustrated in Fig. 2. We then consider the case in which the bare fermion velocities are not equal, i.e.,  $v_z(0) \neq v_p(0)$ . As can be seen from Fig. 2, the relative fixed point of  $u_i/u_2$  is considerably robust against the velocity anisotropy. In particular, the fixed point  $(u_0, u_1, u_2, u_3)/u_2 \approx (0, 0, 1, 0)$  is still present. Clearly, the coupling  $(\Psi^\dagger \tau^y \Psi)^2$  is more important at low energies than the rest three ones.

According to traditional notion, the runaway flow of  $(\Psi^\dagger \gamma^i \Psi)^2$  implies that the system becomes unstable and the fermion bilinear  $\Psi^\dagger \gamma^i \Psi$  acquires a finite vacuum expectation value. However, it has recently becoming clear that this connection might not be always correct [21, 30, 31]. Even if the coupling  $(\Psi^\dagger \tau^y \Psi)^2$  dominates in the low-energy region, the transition driven by nonzero  $(\Psi^\dagger \tau^y \Psi)$  is not necessarily the leading instability. Other instabilities may be more favorable. Moreover, the nonzero  $\langle \Psi^\dagger \tau^y \Psi \rangle$  corresponds to several possible states. One powerful strategy is to consider all of the instabilities at the same time and calculate the energy dependence of all the corresponding susceptibilities [21, 30, 31]. The leading instability should be the one whose susceptibility diverges most rapidly as energy is lowered [21, 30, 31]. It is therefore necessary to take into account all the four types of four-fermion couplings defined in Eq. (2).

The mean value  $\langle \Psi^\dagger \tau^0 \Psi \rangle$  must vanish owing to the particle-hole symmetry. The nonzero mean value  $\langle \Psi^\dagger \tau^z \Psi \rangle$  leads to a shift in the quasiparticle energy. A

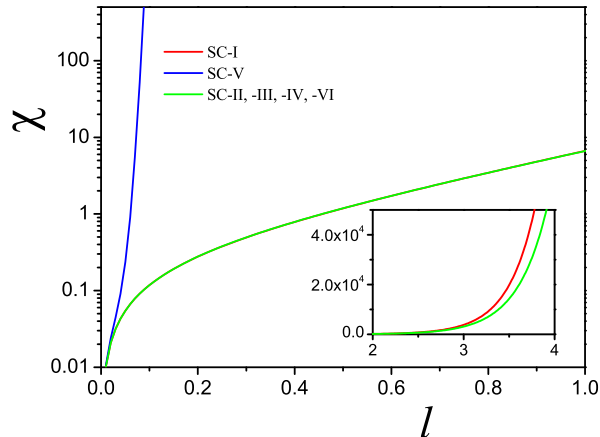


FIG. 3: (Color online) Evolutions of the susceptibilities of all the possible instabilities. We choose  $u_i(0) = 10^{-4}$  for  $i = 0, 1, 2, 3$  and  $v_z(0) = v_p(0) = 0.02$ . Inset: the splitting of susceptibilities that are nearly indistinguishable nearby the leading instability. The basic results are independent of the initial values of fermion velocities and fermion-fermion interactions. The details of these orders are given in Table I.

nonzero  $\langle \Psi^\dagger \tau^x \Psi \rangle$  generates a constant shift to the spin-singlet gap  $\Delta_s$ , which then changes the radius of the gap-vanishing nodal line, but preserves its circular shape. The nonzero mean value  $\langle \Psi^\dagger \tau^y \Psi \rangle$  dynamically breaks the  $\mathcal{T}$ -symmetry, and as such alters the topology.

After performing calculations, we have verified that the generation of nonzero  $\langle \Psi^\dagger \tau^y \Psi \rangle$  is more favorable than the rest ones. However, symmetry consideration allows for six candidate  $\mathcal{TSB}$  SC states [14], as shown in Table I. While in principle each of the six states could occur, only one of them could be realized at low energies. To identify the leading instability, we need to evaluate the susceptibility [16, 17, 30] associated with each possible order as the system approaches the relative fixed point  $(u_0, u_1, u_2, u_3)/u_2 \approx (0, 0, 1, 0)$ . For this purpose, we introduce a source term [16, 21, 32], and write down the following source-related effective action

$$S_{\text{source}} = \int d\tau \int d^3\mathbf{x} \left( \sum_{i=1}^6 \Delta_i \Psi^\dagger \mathcal{M}_i \Psi \right). \quad (11)$$

Here, the concentration is on the charge-channel since the six instabilities are all closely related to the dynamically generated mass term. Each  $\Delta_i$  represents an SC order parameter, and matrix  $\mathcal{M}_i$  specifies how  $\Delta_i$  couples to the fermionic degrees of freedom. The connection between  $\Delta_i$  and  $\mathcal{M}_i$  is summarized in Table I. Combining the effective action (3) and the additional source term (11) yields a renormalized effective action

$$S'_{\text{eff}} = S_{\text{eff}} + S_{\text{source}}. \quad (12)$$

On the basis of Eq. (12), one can directly compute the one-loop corrections to the source strength. We find that

$\Delta_i$  depend on  $l$  as follows

$$\frac{d \ln \Delta_i}{dl} = \mathcal{F}_i(v_z, v_p, u_0, u_1, u_2, u_3, \Delta_i), \quad (13)$$

where the concrete expressions of  $\mathcal{F}_i$  are given in Appendix B. Susceptibilities are computed via the following formula [16, 17, 30, 33]

$$\delta \chi_i(l) = - \frac{\partial^2 \delta f}{\partial \Delta_i(0) \partial \Delta_i^*(0)}, \quad (14)$$

where  $\chi_i$  denotes the susceptibility and  $f(\Delta_i, \Delta_i^*)$  is the free energy functional. The susceptibilities are calculated based on the RG flows of interaction parameters (7)-(10) and fermion velocities (5)-(6), as well as the strength of source terms (13).

Numerical computations show that the leading instability is the transition into  $\mathcal{TSB}$  SC-V state, whose gap symmetry is  $id_{xz}$ -wave. The results are displayed in Fig. 3. When the scale  $l$  grows, the susceptibility of SC-V state increases rapidly and diverges at certain finite value  $l_c$ . As illustrated in the inset of Fig. 3, all the other susceptibilities are still relatively small at  $l_c$ . Notice that the six  $\mathcal{TSB}$  SC states are incompatible: only one can exist at low energies. Once SC-V state is realized, the rest five SC states are excluded. We have verified that this conclusion is insensitive to the starting values of fermion velocities and four-fermion coupling parameters.

A proper extension of our approach may be also applicable to the polar phase of  $^3\text{He}$ . Given the polar phase and phase-A of  $^3\text{He}$  share analogous topological structures of Fermi surfaces with their Phase-I and Phase-II counterparts sketched in Fig. 1 [14, 22], one can realize that principal effective low-energy action of the polar phase of  $^3\text{He}$  is similar to that of 3D line-nodal noncentrosymmetric superconductor. It is therefore natural to expect that the interactions among these gapless quasiparticles excited from nodal points/lines would play a crucial role in pinning down the concrete states in the polar phases once the system undergoes some phase transition from the phase-A to polar phase of  $^3\text{He}$ .

#### IV. SUMMARY

We have studied the impact of short-range four-fermion interactions on the low-energy properties of three-dimensional line-nodal superconductors. In the absence of such short-range interactions, the SC state is topological and has line nodes, which is protected by  $\mathcal{T}$  symmetry. We have found that short-range interactions significantly alter the dynamics of the gapless nodal fermions. Additionally, we have showed that, short-range interactions can lead to dynamical breaking of  $\mathcal{T}$  symmetry, which then changes the topology of the SC state and turns the system into a distinct  $\mathcal{TSB}$  SC phase. After calculating the susceptibilities associated with six candidate  $\mathcal{TSB}$  SC phases, we have demonstrated that the

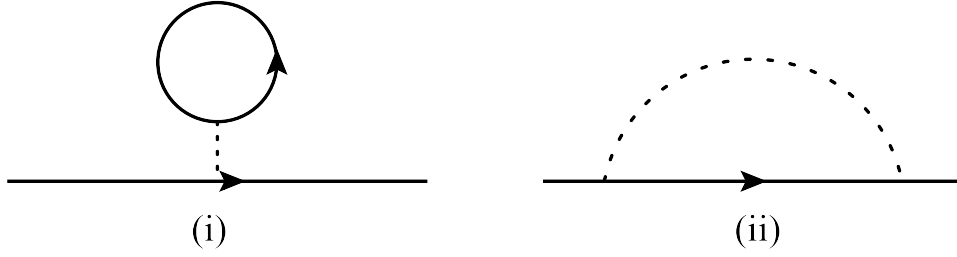


FIG. 4: One-loop corrections to the fermion propagator (the dashed line indicates the interactions).

SC phase with  $\cos(\theta_{\mathbf{k}})\tau^y$  coupling matrix, which amounts to the SC state having  $id_{xz}$ -wave pairing in the noncentrosymmetric case and  $p_z + ip_x$ -wave pairing in the  $p_z$ -polarized case, is the leading instability. We expect that future experiments probe the existence of such a  $\mathcal{T}$ SB SC state in unconventional line-nodal superconductors.

### ACKNOWLEDGEMENTS

I am very grateful to Prof. G. -Z. Liu for providing invaluable comments and kindly polishing this manuscript. In addition, J.W. acknowledges Dr. D.- V. Efremov, and Dr. C. Ortix, as well as Prof. J. van den Brink for correlated collaborations and helpful correspondence. The author would also like to thank Prof. X.-Y. Pan and Miss

Y. -H. Zhai for useful discussions. This work is partially supported by the National Natural Science Foundation of China under Grant No. 11504360.

### Appendix A: One-loop corrections to interaction parameters

Here, we provide details for the one-loop RG calculations. As delineated in Fig. 4 and Fig. 5, the four-fermion interaction contributes to both the fermion self-energy and the four-fermion vertices. The one-loop fermion self-energy is given by Eq. (B5). Hereafter, we focus on the one-loop renormalization of four-fermion vertices. After evaluating the Feynman diagrams shown in Fig. 5, we derive the corrections to vertices as follows,

$$\delta S_{u_0}^{i-v} = \int_{\mathbf{k}_1, \omega_1} \int_{\mathbf{k}_2, \omega_2} \int_{\mathbf{k}_3, \omega_3} \psi^\dagger(\omega_1, \mathbf{k}_1) \tau^0 \psi(\omega_2, \mathbf{k}_2) \psi^\dagger(\omega_3, \mathbf{k}_3) \tau^0 \psi(\omega_1 + \omega_2 - \omega_3, \mathbf{k}_1 + \mathbf{k}_2 - \mathbf{k}_3) \times \left[ \frac{4u_2(u_3\mathcal{E} + u_1\mathcal{F})}{8\pi v_z v_p} l \right], \quad (\text{A1})$$

$$\delta S_{u_1}^{i-v} = \int_{\mathbf{k}_1, \omega_1} \int_{\mathbf{k}_2, \omega_2} \int_{\mathbf{k}_3, \omega_3} \psi^\dagger(\omega_1, \mathbf{k}_1) \tau^1 \psi(\omega_2, \mathbf{k}_2) \psi^\dagger(\omega_3, \mathbf{k}_3) \tau^1 \psi(\omega_1 + \omega_2 - \omega_3, \mathbf{k}_1 + \mathbf{k}_2 - \mathbf{k}_3) \times \left[ \frac{u_1(u_0 + 3u_1 - u_2 - u_3)(\frac{1}{2} + \mathcal{F} - \mathcal{E}) - 2u_2u_3 + 4u_1u_3\mathcal{F}}{8\pi v_z v_p} l \right], \quad (\text{A2})$$

$$\delta S_{u_2}^{i-v} = \int_{\mathbf{k}_1, \omega_1} \int_{\mathbf{k}_2, \omega_2} \int_{\mathbf{k}_3, \omega_3} \psi^\dagger(\omega_1, \mathbf{k}_1) \tau^2 \psi(\omega_2, \mathbf{k}_2) \psi^\dagger(\omega_3, \mathbf{k}_3) \tau^2 \psi(\omega_1 + \omega_2 - \omega_3, \mathbf{k}_1 + \mathbf{k}_2 - \mathbf{k}_3) \times \left[ \frac{u_2(u_0 - u_1 + 3u_2 - u_3)(\frac{1}{2} + \mathcal{E} + \mathcal{F}) - 2u_1u_3 + 4u_2(u_3\mathcal{F} + u_1\mathcal{E})}{8\pi v_z v_p} l \right], \quad (\text{A3})$$

$$\delta S_{u_3}^{i-v} = \int_{\mathbf{k}_1, \omega_1} \int_{\mathbf{k}_2, \omega_2} \int_{\mathbf{k}_3, \omega_3} \psi^\dagger(\omega_1, \mathbf{k}_1) \tau^3 \psi(\omega_2, \mathbf{k}_2) \psi^\dagger(\omega_3, \mathbf{k}_3) \tau^3 \psi(\omega_1 + \omega_2 - \omega_3, \mathbf{k}_1 + \mathbf{k}_2 - \mathbf{k}_3) \times \left[ \frac{u_3(u_0 - u_1 - u_2 + 3u_3)(\frac{1}{2} - \mathcal{F} + \mathcal{E}) - 2u_1u_2 + 4u_3u_1\mathcal{E}}{8\pi v_z v_p} l \right], \quad (\text{A4})$$

with  $\mathcal{E}$  and  $\mathcal{F}$  being designated as

$$\mathcal{E} \equiv \frac{1}{\pi} \int_{-\frac{\pi}{2}}^{\frac{\pi}{2}} d\theta \frac{v_z v_\perp^3 \cos^2 \theta}{(v_z^2 \sin^2 \theta + v_\perp^2 \cos^2 \theta)^{\frac{3}{2}}}, \quad \mathcal{F} \equiv \frac{1}{\pi} \int_{-\frac{\pi}{2}}^{\frac{\pi}{2}} d\theta \frac{v_z^3 v_\perp \sin^2 \theta}{(v_z^2 \sin^2 \theta + v_\perp^2 \cos^2 \theta)^{\frac{3}{2}}}. \quad (\text{A5})$$

### Appendix B: Renormalization group analysis

Within the standard formalism of Wilsonian RG approach [18–20], we need to integrate out the fields defined

in the momentum shell  $b\Lambda < k < \Lambda$ , where  $b < 1$ , to de-



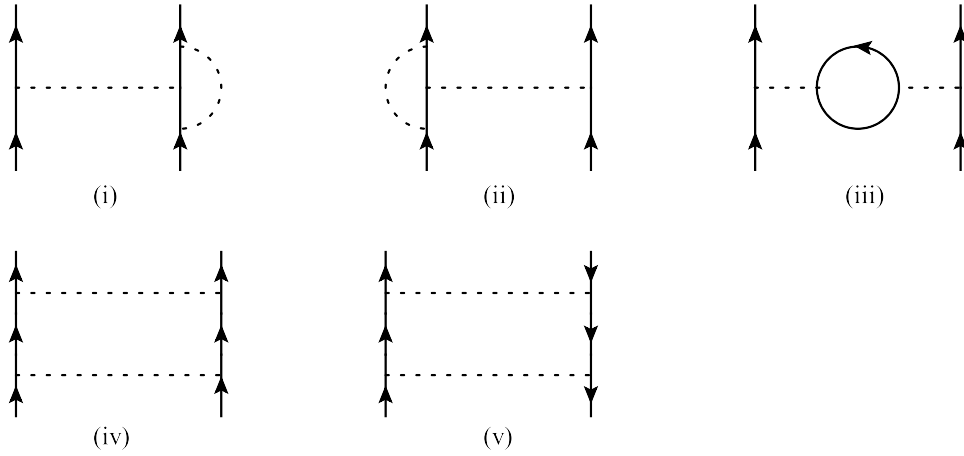


FIG. 5: One-loop corrections to the fermion interacting couplings (the dashed line indicates the interactions).

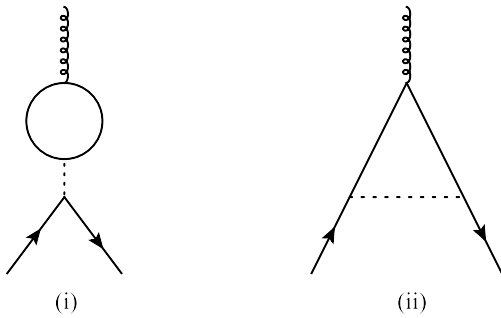


FIG. 6: One-loop corrections to the strength of source terms (the dashed line indicates the interactions).

termine how the interaction parameters of the effective theory (3) evolve upon lowering the energy scale. To proceed, we introduce  $\Lambda$  as the upper energy scale and the variable parameter  $b = e^{-l}$ , where  $l > 0$  is a varying parameter [18–20]. One can re-scale momenta and energy by  $\Lambda_0$ , which is determined by the inverse lattice constant, i.e.  $k \rightarrow k/\Lambda_0$  and  $\omega \rightarrow \omega/\Lambda_0$  [25–27]. This manipulation will help simplify RG calculations.

Before going further, we need to first specify the RG re-scaling transformations. In light of the spirit of momentum-shell RG theory, the  $(-i\omega)$  term in Eq. (3) in the main text can be identified as the free fixed point. Guided by this principle, it is now easy to verify that the momenta, energy and fermion fields should transform as follows [20, 25–27]

$$\omega' = \omega e^{-l}, \quad (\text{B1})$$

$$\delta k'_z = \delta k_z e^{-l}, \quad (\text{B2})$$

$$\delta k'_\perp = \delta k_\perp e^{-l}, \quad (\text{B3})$$

$$\Psi'_{\mathbf{k}',\omega'} = \Psi_{\mathbf{k},\omega} e^{\frac{1}{2} \int_0^l d\ell (4-\eta_f)}. \quad (\text{B4})$$

Here, a parameter  $\eta_f$  is implemented to represent the fermion anomalous dimension, which would be generated by the four-fermion interactions.

Making use of the above definitions, we can perform RG calculation up to the one-loop order. As delineated in Appendix A the four-fermion interactions contribute to both the fermion self-energy and the four-fermion vertex functions. One-loop correction to fermion self-energy is

$$\Sigma(\omega, \mathbf{k}) = \int_{\mathbf{k},\omega} \Psi^\dagger(\omega, \mathbf{k}) \left[ -(u_0 \mathcal{C} l) i\omega \tau_0 - (u_1 \mathcal{C} l) v_p \delta k_\perp \tau^x - (u_3 \mathcal{C} l) v_z \delta k_z \tau^z \right] \Psi(\omega, \mathbf{k}), \quad (\text{B5})$$

where parameter  $\mathcal{C}$  is given by

$$\mathcal{C} = \frac{1}{4\pi v_z v_p}. \quad (\text{B6})$$

Gathering the above self-energy and keeping  $\Psi^\dagger(-i\omega)\Psi$  invariant under RG transformations, we get

$$\eta_f = -\frac{u_0}{4\pi v_z v_p}. \quad (\text{B7})$$

The one-loop contributions to the fermion-source coupling are plotted in Fig. 6. Repeating similar RG procedures, we find that the strength parameters of source terms satisfy the following coupling equations

$$\frac{d \ln \Delta_I}{dl} = \left[ (1 - \eta_f) + \frac{2(u_0 - u_2)(2\mathcal{E} + 2\mathcal{F} + 1) + 2(u_1 + u_3)(2\mathcal{E} + 2\mathcal{F} - 1)}{32\pi v_z v_\perp} \right] \Delta_I, \quad (\text{B8})$$

$$\frac{d \ln \Delta_{II}}{dl} = (1 - \eta_f) \Delta_{II}, \quad (\text{B9})$$

$$\frac{d \ln \Delta_{III}}{dl} = (1 - \eta_f) \Delta_{III}, \quad (\text{B10})$$

$$\frac{d \ln \Delta_{IV}}{dl} = (1 - \eta_f) \Delta_{IV}, \quad (\text{B11})$$

$$\frac{d \ln \Delta_V}{dl} = \left[ (1 - \eta_f) + \frac{4(u_0 - u_2)(\mathcal{E}' + \mathcal{F}' + \mathcal{C}') + 4(u_1 + u_3)(\mathcal{E}' + \mathcal{F}' - \mathcal{C}')}{32\pi v_z v_\perp} \right] \Delta_V, \quad (\text{B12})$$

$$\frac{d \ln \Delta_{VI}}{dl} = (1 - \eta_f) \Delta_{VI}, \quad (\text{B13})$$

with  $\eta_f$  being denominated in Eq. (B7) and  $\mathcal{C}'$ ,  $\mathcal{E}'$ ,  $\mathcal{F}'$  introduced as

$$\mathcal{C}' = \frac{1}{\pi} \int_{-\frac{\pi}{2}}^{\frac{\pi}{2}} d\theta \frac{v_z v_\perp \cos \theta}{\sqrt{v_z^2 \sin^2 \theta + v_\perp^2 \cos^2 \theta}}, \quad (\text{B14})$$

$$\mathcal{E}' = \frac{1}{\pi} \int_{-\frac{\pi}{2}}^{\frac{\pi}{2}} d\theta \frac{v_z v_\perp^3 \cos^3 \theta}{(v_z^2 \sin^2 \theta + v_\perp^2 \cos^2 \theta)^{\frac{3}{2}}}, \quad (\text{B15})$$

$$\mathcal{F}' = \frac{1}{\pi} \int_{-\frac{\pi}{2}}^{\frac{\pi}{2}} d\theta \frac{v_z^3 v_\perp \cos \theta \sin^2 \theta}{(v_z^2 \sin^2 \theta + v_\perp^2 \cos^2 \theta)^{\frac{3}{2}}}. \quad (\text{B16})$$

Here, the strength of source terms  $\Delta_i$  with  $i = 1 - 9$  is presented in Table I of the main text.

- 
- [1] J. Bardeen, L. N. Cooper, and J. R. Schrieffer, *Phys. Rev.* **108**, 1175 (1957).
- [2] M. Tinkham, *Introduction to Superconductivity*, *Dover Books on Physics Series*, Dover Publications, 1996.
- [3] P. A. Lee, N. Nagaosa, and X.-G. Wen, *Rev. Mod. Phys.* **78**, 17 (2006).
- [4] M. Vojta, Y. Zhang, and S. Sachdev, *Phys. Rev. Lett.* **85**, 4940 (2000); M. Vojta, *Rep. Prog. Phys.* **66**, 2069 (2003).
- [5] T. Valla, A. Fedorov, P. Johnson, B. Wells, S. Hulbert, Q. Li, G. Gu, and N. Koshizuka, *Science* **285**, 2110 (1999).
- [6] I. Bonalde, W. Brammer-Escamilla, and E. Bauer, *Phys. Rev. Lett.* **94**, 207002 (2005).
- [7] K. Izawa, Y. Kasahara, Y. Matsuda, K. Behnia, T. Yasuda, R. Settai, and Y. Onuki, *Phys. Rev. Lett.* **94**, 197002 (2005).
- [8] A. Gasparini, Y. Huang, N. Huy, J. Klaasse, T. Naka, E. Slooten, and A. De Visser, *J. of Low Tem. Physics* **161**, 134 (2010).
- [9] J.-P. Reid, M. Tanatar, X. Luo, H. Shakeripour, N. Doiron-Leyraud, N. Ni, S. Budko, P. Canfield, R. Prozorov, and L. Taillefer, *Phys. Rev. B* **82**, 064501 (2010).
- [10] M. Tanatar, J.-P. Reid, H. Shakeripour, X. Luo, N. Doiron-Leyraud, N. Ni, S. Budko, P. Canfield, R. Prozorov, and L. Taillefer, *Phys. Rev. Lett.* **104**, 067002 (2010).
- [11] M. Sigrist and K. Ueda, *Rev. Mod. Phys.* **63**, 239 (1991).
- [12] Y. Matsuda, K. Izawa, and I. Vekhter, *J. Phys. Condens. Matter* **18**, R705 (2006).
- [13] S. Matsuura, P.-Y. Chang, A. P. Schnyder, and S. Ryu, *New J. Phys.* **15**, 065001 (2013).
- [14] S. E. Han, G. Y. Cho, and E. G. Moon, *Phys. Rev. B* **95**, 094502 (2017).
- [15] K. Sun, H. Yao, E. Fradkin, and S. A. Kivelson, *Phys. Rev. Lett.* **103**, 046811 (2009).
- [16] J. M. Murray and O. Vafek, *Phys. Rev. B* **89**, 201110(R) (2014).
- [17] J. Wang, C. Ortix, J. van den Brink, and D. V. Efremov, *Phys. Rev. B* **96**, 201104(R) (2017).
- [18] K. G. Wilson, *Rev. Mod. Phys.* **47**, 773 (1975).
- [19] J. Polchinski, arXiv: hep-th/9210046 (1992).
- [20] R. Shankar, *Rev. Mod. Phys.* **66**, 129 (1994).
- [21] A. V. Chubukov, M. Khodas, and R. M. Fernandes, *Phys. Rev. X* **6**, 041045 (2016).
- [22] G. E. Volovik, *The Universe in a Helium Droplet*, (Oxford University Press, Oxford, 2003).
- [23] P. Frigeri, D. Agterberg, A. Koga, and M. Sigrist, *Phys. Rev. Lett.* **92**, 097001 (2004).
- [24] P. Brydon, A. P. Schnyder, and C. Timm, *Phys. Rev. B* **84**, 020501 (2011).
- [25] Y. Huh and S. Sachdev, *Phys. Rev. B* **78**, 064512 (2008).
- [26] J.-H. She, J. Zaanen, A. R. Bishop, and A. V. Balatsky, *Phys. Rev. B* **82**, 165128 (2010).
- [27] J. Wang, G.-Z. Liu, and H. Kleinert, *Phys. Rev. B* **83**, 214503 (2011).
- [28] J. Wang, *J. Phys. Condens. Matter* **30**, 125401 (2018).
- [29] J. Wang, A. Eberlein, and W. Metzner, *Phys. Rev. B* **89**, 121116(R) (2014).
- [30] V. Cvetkovic, R. E. Throckmorton, and O. Vafek, *Phys. Rev. B* **86**, 075467 (2012).
- [31] C. J. Halboth and W. Metzner, *Phys. Rev. Lett.* **85**, 5162 (2000); C. J. Halboth and W. Metzner, *Phys. Rev. B* **61**, 7364 (2000).

- [32] S. Maiti and A. V. Chubukov, Phys. Rev. B **82**, 214515 (2010).
- [33] D. R. Nelson, Phys. Rev. B **11**, 3504 (1975).